


# Static and dynamical Stark many-body localization transition in a linear potential

Xingbo Wei <sup>1,2</sup> Xianlong Gao <sup>3</sup> and W. Zhu<sup>2,\*</sup>

<sup>1</sup>Department of Physics, Zhejiang University, Hangzhou 310027, China

<sup>2</sup>Key Laboratory for Quantum Materials of Zhejiang Province, School of Science, Westlake University, Hangzhou 310024, China

<sup>3</sup>Department of Physics, Zhejiang Normal University, Jinhua 321004, China



(Received 5 May 2022; revised 28 June 2022; accepted 7 October 2022; published 21 October 2022)

We investigate hard-core bosons filled in a lattice chain in the presence of a weak linear potential. In the single-particle case, we find that the critical point of dynamical Stark localization is different from that of static Stark localization. This suggests an intermediate phase in which the eigenstates are Stark-localized, but the dynamic wave functions are extended after quenching. In the many-body case, by comparing the dynamical critical point with the static critical point, we find a many-body intermediate phase that is analogous to the single-particle intermediate phase. Furthermore, we also study the static transition for the ground state and the dynamical transition for domain-wall states. In the ground state, we find that the localization transition point is at  $V \approx 2(U + W)$  for half-filling ( $U$  is the nearest-neighbor interaction strength,  $W$  is the half-bandwidth). For the typical domain-wall state  $|111 \dots 000\rangle$ , its dynamical transition points are at  $V \approx 4(U + W)$  and  $V \approx 4(U - W)$ . By analyzing the distribution of the occupation, we also offer a phenomenological way to estimate the above transition points.

DOI: [10.1103/PhysRevB.106.134207](https://doi.org/10.1103/PhysRevB.106.134207)

## I. INTRODUCTION

The phenomenon of many-body localization (MBL), strong disorder breaking ergodicity in the isolated quantum system, has received extensive attention in the past few years [1–6]. This topic has forged many interesting directions in quantum information [7–10] and out-of-equilibrium statistical mechanics [2–4, 11–18]. Although a great deal of fundamental work has been explored [2–5], limited by the computational ability, many issues are still under debate, e.g., the many-body mobility edge (MBE) [19–21] and the many-body intermediate phase (MBI) [22–25], and even MBL itself has been questioned in the past two years [26–28]. Nonetheless, it is undeniable that MBE, MBI, and MBL have indeed been observed in finite-size systems [19–28].

Recently, it has been shown that disorder is not necessary for MBL [29–31], i.e., it can be generated in disorder-free systems. Typically, the strong linear potential can cause MBL, dubbed as Stark many-body localization (SMBL) [30, 31]. SMBL can be considered as a generalization of Wannier-Stark localization to the many-body case [32], which has a different mechanism from MBL. Although the origins are different, the similarity between SMBL and MBL allows several theoretical methods used in disordered systems to be applied to study SMBL, e.g., level statistics [30, 31], dynamical behavior [33–35], entanglement entropy [34–38], and so on. In addition to theoretical investigations, there are a lot of experimental studies on SMBL [39–43]. In particular, recent experiments show that SMBL can be realized using quantum simulations [39–42].

Previous studies have shown that an ergodic-SMBL transition occurs when the amplitude of the ordered potential increases [30, 31, 44], which is similar to the ergodic-MBL transition in disordered systems. This ergodicity was considered as a “strong” one [30, 31, 44]. Here, “strong” means that the ergodic phase satisfies the eigenstate thermalization hypothesis (ETH) [45–47], which implies that the long-time behavior of the local observation does not depend on the choice of the initial state. However, in their latest work, Doggen *et al.* found that the ergodicity in the system with a linear potential is not a “strong” one [48]. They found that the domain-wall states keep local information after long-time evolution even for a weak linear potential. This manifests that, although most initial states lose memory after time evolution, a small part of the initial states can retain local information without approaching thermalization. Meanwhile, it also means that the local constraints make the Hilbert space fragment into disconnected sectors, and the Hilbert space is shattering [49, 50].

In a single-particle system with a strong linear potential  $V_i$ , where  $V$  is the slope and  $i$  is the site index, the amplitude of the potential  $\Delta V = V_{\max} - V_{\min} = VL$  increases with size. It is well known that all states are Wannier-Stark localized states for any finite  $V$  in the thermodynamic limit for  $L \rightarrow \infty$  [31, 51]. However, it also shows that there are extended states in a system with a weak linear potential [52]. The transition from extended states to Wannier-Stark localized (bound) states is dubbed the transition from the classically allowed region to the classically forbidden region [53], which is determined by the eigenvalue and the amplitude of the linear potential  $\Delta V$ , as shown in Fig. 1(a). Thus, it is necessary to use a weak linear potential with a finite  $\Delta V$  to study the localization transition. Note that the localization here, which

\*zhuwei@westlake.edu.cn

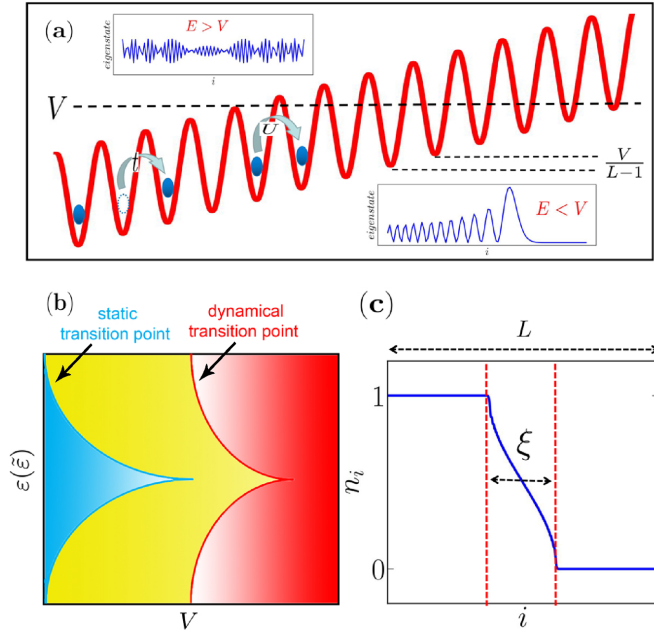


FIG. 1. (a) Schematic plot of hard-core bosons in a linear potential. The minimum value of the linear potential is  $V_{\min} = 0$ , and the maximum value is  $V_{\max} = V$ , so the gap between two nearest-neighbor sites is  $V/(L-1)$ . When the eigenvalue  $E$  is larger than the maximum value of the linear potential  $E > V$ , the corresponding eigenstate behaves as a scattering extended state. On the contrary, the eigenstate is a Stark-localized state when  $E < V$ . (b) Schematic plot of the intermediate phase in the single-particle case. The blue, yellow, and red regions represent static and dynamical extended (extended), static localized but dynamical extended (intermediate), and static and dynamical localized (localized) phases, respectively. (c) Typical occupation  $n_i$  and the lengthscale  $\xi$  denoting the width of the region  $0 < n_i < 1$ .

is defined as the Wannier-Stark localization length  $\xi_{\text{loc}}$ , is smaller than the system size  $L$  [52,54–56]. Different from the localization length in the disordered system, the localization length in a system with an ordered potential characterizes the distribution width of the wave function [54,55]. For  $\xi_{\text{loc}} < L$ , the wave function is localized (bound). On the contrary, the wave function is extended for  $\xi_{\text{loc}} > L$  [52,54–56]. In the many-body case, our results below show that the weak linear potential is especially important for the ground state and domain-wall states. In this paper, we determine that there is an intermediate phase in the process of the SMBL transition by comparing critical points in the static and dynamical cases. To the best of our knowledge, it has not been studied before. Furthermore, we also study the static transition for the ground state and the dynamical transition for domain-wall states. Due to the interaction, the analytical solution becomes difficult. However, interestingly, we find that the specific formulas of the lengthscale  $\xi$  denoting the width of the region  $0 < n_i < 1$ , as shown in Fig. 1(c), can be obtained by analyzing the occupation distribution. The lengthscale  $\xi$  is proposed to distinguish Stark many-body localization for domain-wall initial states in Refs. [48,62]. Our results shown in Appendix C indicate that it is suitable for distinguishing not only the localization of domain-wall initial states but also the

localization of the ground state. The criterion of localization and delocalization is that the state is in the localization phase for  $\xi < L$ , whereas the state is in the delocalization phase for  $\xi > L$  [48,62]. In this work, we systematically study the effects of the linear potential and the interaction on  $\xi$ , and we obtain the transition points.

The paper is organized as follows. In Sec. II, we introduce a one-dimensional hard-core-boson model with a linear potential. In Sec. III, we study the static and dynamical localization in the single-particle case. In Sec. IV, we map the single-particle to many-body states and study the static and dynamical localization in the middle of the spectrum. Furthermore, we also investigate the static localization in the ground state and the dynamical localization of different domain-wall initial states in this section. Finally, we summarize our conclusions in Sec. V.

## II. MODEL

We consider a one-dimensional hard-core boson model with  $L$  sites, which reads

$$\hat{H} = -t \sum_{(i,j)} (\hat{b}_i^\dagger \hat{b}_j + \text{H.c.}) + U \sum_i \hat{n}_i \hat{n}_{i+1} + \sum_{i=0}^{L-1} V_i \hat{n}_i, \quad (1)$$

where  $\hat{b}_i^\dagger$  ( $\hat{b}_i$ ) creates (eliminates) a hard-core boson at the site  $i$ ,  $(\hat{b}_i^\dagger)^2 = 0$ .  $\hat{n}_i = \hat{b}_i^\dagger \hat{b}_i$  is the occupation number operator,  $t \equiv 1$  denotes the hopping energy,  $U$  represents the strength of the nearest-neighbor interaction, and  $V_i$  is the amplitude of the potential. Here we use a linear potential  $V_i = V \frac{i}{L-1}$ , which has a minimum value  $V_{\min} = 0.0$  and a maximum value  $V_{\max} = V$ .

For Eq. (1), it is well known that all states are Wannier-Stark localized states in the thermodynamic limit when the potential is shown as  $V_i = Fi$  [31]. It should be emphasized that  $F$  in Ref. [31] is equivalent to  $\frac{V}{L-1}$  in our paper. In the absence of the linear potential, the ground state of the model can be solved by using the Bethe ansatz, and it shows a gapped phase separation (PS) for  $U/t \leq -2.0$  [57]. Furthermore, Eq. (1) maps to the isotropic Heisenberg model via a Matsubara-Matsuda mapping for  $U/t = 2$  and  $V_i/t = 0$  [58], showing as an integrable system [45,59].

## III. SINGLE-PARTICLE CASE

We first consider the single-particle case with the particle number  $N = 1$ . To obtain the single-particle localization transition point, one may regard the ordered potential as a barrier as shown in Fig. 1(a). When the eigenvalue is smaller than the energy of the barrier, the eigenstate is a Stark-localized state (bound state). On the contrary, the eigenstate appears as a scattering extended state when the eigenvalue is larger than the energy of the barrier. Thus, we can easily obtain energies of mobility edges as

$$\begin{aligned} E_{c1}/t &= -W/t + V_{\max}/t, \\ E_{c2}/t &= W/t + V_{\min}/t, \end{aligned} \quad (2)$$

where  $W = 2t$  is the half-width of a band with the particle-hole symmetry.  $V_{\min}$  ( $V_{\max}$ ) is the minimum (maximum) value of the ordered potential. Considering  $V_i = V \frac{i}{L-1}$ , one can see that mobility edges are at  $E_{c1}/t = -2.0 + V/t$

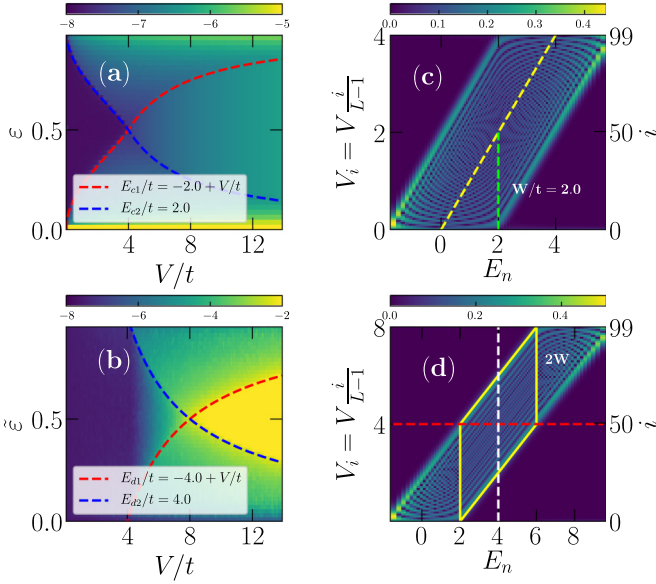


FIG. 2. The phase diagram of static Stark localization in (a) and that of dynamical Stark localization in (b). Parts (c) and (d) show the eigenstates for  $V/t = 4.0$  and  $8.0$ , respectively. Here we use  $L = 4000$  in (a), (b) and  $L = 100$  in (c), (d). The boundary condition is the periodic boundary condition. In the left panels,  $\varepsilon = n/(L-1)$  in (a) is the energy level density, where  $n$  represents the  $n$ th eigenstate, and  $\tilde{\varepsilon} = j/(L-1)$  in (b) is the energy level density of dynamics, where  $j$  represents the initial position of the boson in the initial state. In the right panels, the right ordinate represents the site  $i$ , and the corresponding local potential energy  $V_i = V i/(L-1)$  is shown on the left. The color stands for  $\ln(\text{IPR}^{(n)})$  in (a) and  $\ln(\text{IPR}_{\mathcal{T}=10,000.5\mathcal{T}_b})$  with the Bloch period  $\mathcal{T}_b = \frac{2\pi(L-1)}{V}$  in (b), where  $\text{IPR}^{(n)} = \sum_i |c_i^n|^4$  and  $\text{IPR}_{\mathcal{T}} = \sum_i |\psi_i(j, \mathcal{T})|^4$ . The color in (c), (d) is  $|c_i^n|^4$ .

and  $E_{c2}/t = 2.0$ . In Fig. 2(a), we adopt the inverse participation ratio  $\text{IPR}^{(n)} = \sum_i |c_i^n|^4$  to indicate the transition, where  $c_i^n = \langle i|n \rangle$  is the coefficient obtained by expanding eigenstates  $|n\rangle$  with basis vectors  $|i\rangle$ . The color represents  $\ln(\text{IPR}^{(n)})$ , which changes significantly on the mobility edges. By examining eigenstates, we confirm that eigenstates with eigenvalues  $E_{c1} < E < E_{c2}$  are scattering extended states, whereas eigenstates with eigenvalues  $E < E_{c1}$  and  $E > E_{c2}$  are Stark-localized states. Furthermore, one can also obtain that the Stark localization transition point is at  $V/t = 4.0$  with  $E_{c1}/t = E_{c2}/t$ . When the amplitude  $V/t > 4.0$ , all states are Stark-localized states in the spectrum. The distribution of eigenstates  $|c_i^n|$  for  $V/t = 4.0$  is shown in Fig. 2(c), in which the abscissa  $E_n$  represents the  $n$ th eigenvalue, the ordinate  $i$  on the right is the site index, and the corresponding local potential energy  $V_i = Vi/(L-1)$  is on the left ordinate. The distribution of eigenstates has a center with local potential energy  $V_i = E_n$  [the yellow dotted line in Fig. 2(c)] with a half-width  $W/t = 2$  [the green dotted line in Fig. 2(c)].

Next we turn to investigate the dynamical Stark localization transition. We consider an initial state  $|\psi(j, \mathcal{T} = 0)\rangle$ , where  $j$  represents the local position of the single particle at the time  $\mathcal{T} = 0$ . The energy of the initial state is  $V_j = Vj/(L-1)$ , which is  $j$ -dependent. This initial state can be expanded by eigenstates  $|n\rangle$  as  $|\psi(j, \mathcal{T} = 0)\rangle = \sum_n c_i^n |n\rangle$ .

Meanwhile,  $|n\rangle$  can also be expanded by basis vectors  $|i\rangle$  as  $|n\rangle = \sum_i c_i^n |i\rangle$ . Thus the wave function after time evolution reads

$$\begin{aligned} |\psi(j, \mathcal{T})\rangle &= e^{-i\hat{H}\mathcal{T}} |\psi(j, \mathcal{T} = 0)\rangle \\ &= \sum_i \sum_n c_i^n c_j^n e^{-iE_n\mathcal{T}} |i\rangle \equiv \sum_i \psi_i(j, \mathcal{T}) |i\rangle, \end{aligned} \quad (3)$$

where  $E_n$  is from  $\hat{H}|n\rangle = E_n|n\rangle$ .  $\psi_i(j, \mathcal{T}) = \sum_n c_i^n c_j^n e^{-iE_n\mathcal{T}}$  indicates that once  $c_i^n c_j^n = 0$  for any  $n$ , the coefficient  $\psi_i(j, \mathcal{T}) = 0$ . Meanwhile, it also implies that the dynamical localization transition point could be obtained by analyzing the distribution of eigenstates. We show typical eigenstates  $|c_i^n|$  for  $V/t = 8.0$  in Fig. 2(d), and we choose an initial state with  $j = L/2$  and  $V_j \approx 4.0$ . The red dotted line represents that the initial state is expanded by eigenstates  $|\psi(j, \mathcal{T} = 0)\rangle = \sum_n c_i^n |n\rangle$ , and the white dotted line as an example denotes that the eigenstate with the eigenvalue  $E_n/t = 4.0$  is expanded by basis vectors  $|n\rangle = \sum_i c_i^n |i\rangle$ . By expanding the initial state and eigenstates, one can find a region with  $c_i^n c_j^n \neq 0$  surrounded by yellow lines in Fig. 2(d), and the remaining region with  $c_i^n c_j^n = 0$ . The vertical width of the region of  $c_i^n c_j^n \neq 0$  is  $2W/t = 4$ , which is equal to the width of the band. Obviously, all basis vectors are exactly covered in the region enclosed by yellow lines for  $V/t = 8.0$ , thus one may expect that all basis vectors can be populated after quenching. Tuning the local potential energy of the initial state  $E_d = V_j/t$  by shifting the red dotted line in Fig. 2(d), we can obtain that the wave function after time evolution can just touch the boundary of the ordered potential when the energy of the initial state satisfies  $E_d/t + 2W/t = V_{\max}/t$  or  $E_d/t - 2W/t = V_{\min}/t$ , which yields dynamical mobility edges

$$\begin{aligned} E_{d1}/t &= V_{\max}/t - 2W/t, \\ E_{d2}/t &= V_{\min}/t + 2W/t. \end{aligned} \quad (4)$$

In our typical case, dynamical mobility edges are at  $E_{d1}/t = V/t - 4.0$  and  $E_{d2}/t = 4.0$  as shown in Fig. 2(b), in which the wave function is localized for  $E_d/t < V/t - 4$  and  $E_d/t > 4$ , whereas it is extended for  $V/t - 4 < E_d/t < 4$ . Similar to the static case, we can also get that the dynamical localization transition point is at  $V_d/t = 8.0$  with  $E_{d1}/t = E_{d2}/t$ . Interestingly, this dynamical localization transition point is not the same as the static one, indicating that there is an intermediate phase. The schematic plot of this phase is shown in Fig. 1(b), and more details are shown in Appendix A. In this intermediate phase, eigenstates are Stark-localized states, but quenched wave functions are extended. Furthermore, one can also find that an arbitrary initial state can (cannot) populate all the basis vectors after quenching for  $V/t < 4.0$  ( $V/t > 8.0$ ), whereas the long-time behavior depends on the choice of the initial state for  $4.0 < V/t < 8.0$ .

Before entering the many-body section, we investigate a noninteracting system with  $N = L/2$  hard-core bosons. Due to the interaction  $U/t = 0$ , this system is essentially a single-particle system. In Fig. 3(a), we show a schematic extracted from the probability density  $|c_i^n|^2$  for  $V/t = 16$  and  $L = 1000$ , which is similar to  $|c_i^n|$  in Figs. 2(c) and 2(d), but the abscissa and ordinate are exchanged. The region surrounded by yellow lines represents  $|c_i^n|^2 \neq 0$ , which has a center at  $V_i = E_n$  (the yellow dotted line) with a half-width  $W/t = 2.0$

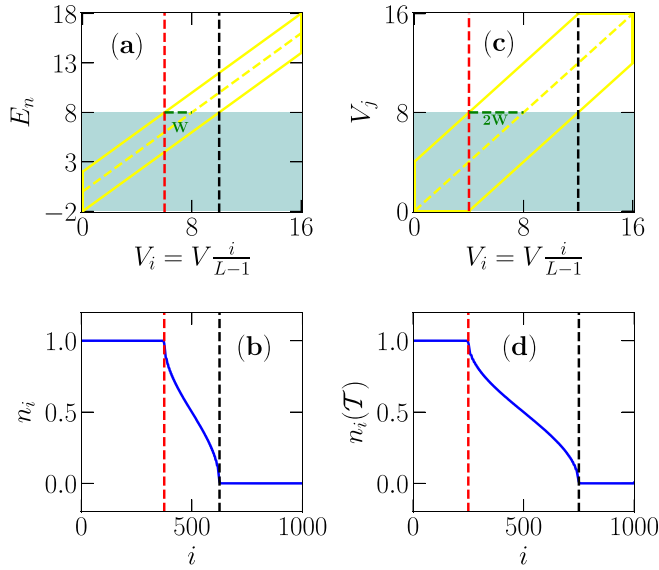


FIG. 3. (a) A schematic extracted from the probability density  $|c_i^n|^2$ . (b) The ground-state density  $n_i$ . (c) A schematic extracted from wave function  $|\psi_i(j, \mathcal{T})|^2$ . (d) The density  $n_i(\mathcal{T})$  for  $\mathcal{T}/t = 10\,000$ . The red and black dotted lines in the upper panel correspond to those in the lower panel one-to-one.  $L = 1000$ ,  $U/t = 0$ , and  $V/t = 16$ .

(the green dotted line), and the remaining region is  $|c_i^n|^2 = 0$ . In the ground state with half-filling, states with energy  $E/t \leq E_n/t \approx 8$  are filled, which is covered by the teal shadow. The eigenstates are unitary,  $UU^\dagger = U^\dagger U = 1$ , thus one can obtain  $\sum_n |c_i^n|^2 = 1$ . The density of  $N$  hard-core bosons is  $n_i = \sum_{n=0}^{N-1} |c_i^n|^2$ , which is equal to 1 when the teal shadow covers all  $|c_i^n|^2 \neq 0$ . On the contrary,  $n_i = 0$  when the teal shadow only covers  $|c_i^n|^2 = 0$ . This is confirmed by Fig. 3(b), in which we show the density  $n_i$  in the ground state for half-filling. The red and black dotted lines correspond to those in Fig. 3(a) one-to-one. The local potential energy of the red dotted line at  $i = 375$  is  $V_i/t \approx 6$  and that of the black dotted line at  $i = 624$  is  $V_i/t \approx 10$ . Then we study the dynamical behavior of the domain-wall state  $|111 \dots 000\rangle$  with half-filling,  $N = L/2$ . In the initial state, sites for  $0 \leq j \leq N - 1$  are occupied. We show a schematic extracted from  $|\psi_i(j, \mathcal{T})|^2$  in Fig. 3(c). The ordinate  $V_j$  is the local potential energy of the boson at the site  $j$  in the domain-wall state. Similar to Fig. 3(a), the yellow lines surround  $|\psi_i(j, \mathcal{T})|^2 \neq 0$  and the remaining region is  $|\psi_i(j, \mathcal{T})|^2 = 0$ , and the distribution of  $|\psi_i(j, \mathcal{T})|^2$  has a center at  $V_i = V_j$  with a half-width  $2W$ . Here, the half-width in the dynamical case in Fig. 3(c) is twice that in the static case in Fig. 3(a), which is the same as the cases shown in Figs. 2(c) and 3(d). The teal shadow covers  $|\psi_i(j, \mathcal{T})|^2$  for  $0 \leq j \leq N - 1$  with energy  $V_j/t \leq V_{j=N-1}/t \approx 8$  due to sites for  $0 \leq j \leq N - 1$  being occupied in the domain-wall initial state. Since  $\sum_j |\psi_i(j, \mathcal{T})|^2 = 1$  obtained from the unitarity, one can obtain that the density after time evolution  $n_i(\mathcal{T}) = \sum_{j=0}^{N-1} |\psi_i(j, \mathcal{T})|^2 = 1$  when the teal shadow covers all  $|\psi_i(j, \mathcal{T})|^2 \neq 0$ . On the contrary,  $n_i(\mathcal{T}) = 0$  when the teal shadow only covers  $|\psi_i(j, \mathcal{T})|^2 = 0$ . This is evidenced by Fig. 3(d), in which the density corresponding to Fig. 3(c) shows that  $n_i = 1$  for  $i < 250$  and  $n_i = 0$  for  $i > 750$ .

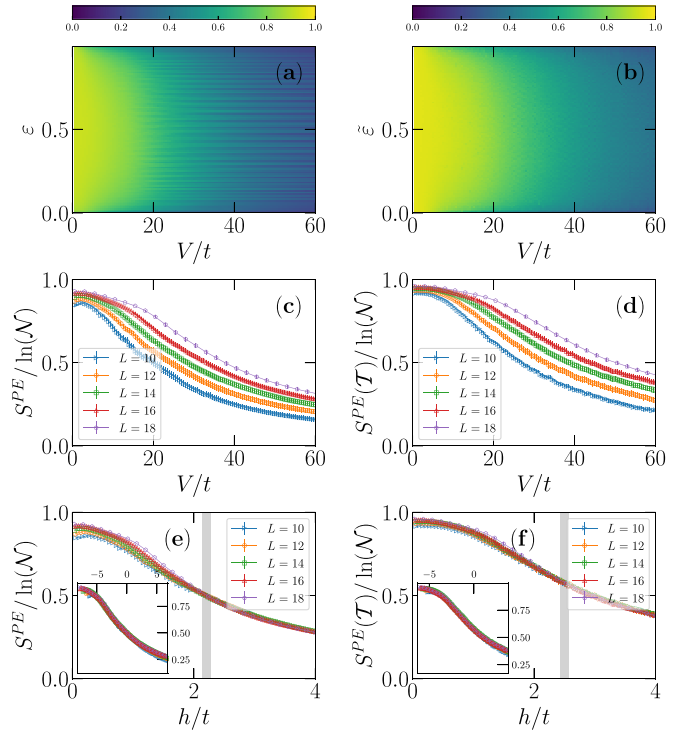


FIG. 4. Color plot of (a) static  $S^{\text{PE}}/\ln \mathcal{N}$  and (b) dynamical  $S^{\text{PE}}(\mathcal{T})/\ln \mathcal{N}$ . In (a), (b),  $L = 16$ . (c)  $S^{\text{PE}}$  for  $\varepsilon \approx 0.5$  and (d)  $S^{\text{PE}}(\mathcal{T})$  for  $\varepsilon \approx 0.5$  as a function of  $V$ . (e)  $S^{\text{PE}}$  for  $\varepsilon \approx 0.5$  and (f)  $S^{\text{PE}}(\mathcal{T})$  for  $\varepsilon \approx 0.5$  as a function of  $h$ , by fixing  $U/t = 1.0$ . In (b), (d), (f),  $\mathcal{T}/t = 10\,000$  and initial states are arranged in ascending order of potential energy. In (c), (d), (e), (f), error bars are from the different samples by adding a weakly disordered perturbation to the linear potential.

#### IV. MANY-BODY CASE

In the previous section, we studied the properties of the noninteracting system. Now let us consider an interacting case  $U \neq 0$  with  $N$  hard-core bosons. First, we study the static and dynamical transitions in the middle of the spectrum by using exact diagonalization (ED). Secondly, we study the transition in the ground state by means of the density matrix renormalization group (DMRG) algorithm [60,61]. Finally, we also investigate the dynamical transition for different domain-wall initial states by ED. The criterion of the localization for the ground-state and domain-wall states is  $\xi < L$  [48,62], i.e., the lengthscale denoting the width of the region  $0 < n_i < 1$  is smaller than the system size, as shown in Fig. 1(c). On the contrary, the state is in the delocalization phase for  $\xi > L$ . The lengthscale  $\xi$  is an important quantity in Refs. [48,62], but it still lacks quantitative analysis. In this section, we systematically study the effects of the linear potential and the interaction on  $\xi$ , and we seek transition points.

##### A. Many-body intermediate phase

In Figs. 4(a) and 4(b), we adopt the participation entropies  $S^{\text{PE}} = -\sum_i |c_i^n|^2 \ln |c_i^n|^2$  [12] and time-dependent participation entropies  $S^{\text{PE}}(\mathcal{T}) = -\sum_j |\psi_i(j, \mathcal{T})|^2 \ln |\psi_i(j, \mathcal{T})|^2$  to study the static and dynamical transitions, respectively. In the calculation, we arrange the basis vectors in ascending order

of potential energy, and  $j$  in  $\psi_i(j, \mathcal{T})$  indicates that we use the  $j$ th basis vector as the initial state. It is expected that, for static (dynamical) perfectly delocalized states  $S^{\text{PE}}/\ln \mathcal{N} = 1.0$  [ $S^{\text{PE}}(\mathcal{T})/\ln \mathcal{N} = 1.0$ ], where  $\mathcal{N}$  is the dimension of the Hilbert space. In contrast,  $S^{\text{PE}}(S^{\text{PE}}(\mathcal{T})) = \text{const}$  for localized states. In Figs. 4(a) and 4(b), both static and dynamical phase diagrams exhibit that the ergodicity region has a “D” shape, suggesting the existence of many-body mobility edges in finite-size systems [35,63]. Using the same color bar, one can find that the ergodicity region in (b) is slightly larger than that in (a). To show more details, we fix  $\varepsilon \approx 0.5$  and  $\bar{\varepsilon} \approx 0.5$  to study  $S^{\text{PE}}$  and  $S^{\text{PE}}(\mathcal{T})$  for different  $V$  in Figs. 4(c) and 4(d), in which  $S^{\text{PE}}(\mathcal{T}) > S^{\text{PE}}$  for the same parameters, indicating that the dynamical wave function is closer to the perfectly delocalized state. Note that the curves for different sizes do not form intersections as  $V$  increases in Figs. 4(c) and 4(d) due to the fact that the transition point shifts with the size [64]. Following the work with strong linear potentials [31], we rewrite the potential amplitude by defining  $h = V/(L-1)$ . In Fig. 4(e), different curves intersect at  $h/t \approx 2.2$ , which is slightly smaller than the intersection at  $h/t \approx 2.5$  in Fig. 4(f). This difference indicates the existence of a many-body intermediate phase within  $2.2 < h < 2.5$  in the middle of the spectrum. In the insets of Figs. 4(e) and 4(f), we employ the ansatz  $f[(h-h_c)L^{1/\nu}]$  to scale finite-size data. The exponents  $\nu \approx 2.17$  in (e) and  $\nu \approx 3.09$  in (f) obey the Harris-Chayes-Chayes-Fisher-Spencer (Harris-CCFS) bound  $\nu \geq 2/d$  [38,65,66], where  $d$  is the dimension of the system. Importantly, different from the many-body intermediate phase with nonergodic delocalized many-body states [22–25], the many-body intermediate phase here shows the dynamical extension but static localization.

## B. Ground state

In Fig. 5(a), we show the distribution of  $\delta n_i(N) = n_i(N+1) - n_i(N)$  for  $U/t = 1$  and  $V/t = 14$ , where  $n_i(N)$  is the ground-state density of  $N$  hard-core bosons. Here we also introduce the gap as  $\delta E(N) = E_0(N+1) - E_0(N)$ , where  $E_0(N)$  is ground-state energy. The ordinate  $\delta E(N) - U$  represents the energy excluding the interaction. The added hard-core boson tends to form double occupation with two nearest-neighbor sites in the ground state, thus the interaction term provides energy  $U$ . For convenience, we define  $E_{\text{center}} = \delta E(N) - U$ . The distribution of  $\delta n_i(N)$  is similar to  $|c_i^n|^2$  in the noninteracting case in Fig. 3(a), which has a center at  $\delta E(N) - U = V_i$  (the yellow dotted line) with a half-width  $(W+U)/t = 3$  (the white dotted line). This half-width is larger than that in Fig. 3(a) due to the fact that the interaction sets in an additional energy cost for double occupation two nearest-neighbor sites. We fix the filling factor  $\rho = N/L = 0.5$  (other filling cases are shown in Appendix B). Similar to the analysis in Fig. 3(a), the states with energy lower than  $E_{\text{center}}/t = [\delta E(L/2) - U]/t \approx 7$  (the cyan dotted line) are filled for half-filling, thus one can obtain that sites with local potential energy  $V_i/t < [E_{\text{center}}/t - (W+U)/t] = 4$  are fully occupied, whereas those with local potential energy  $V_i/t > [E_{\text{center}}/t + (W+U)/t] = 10$  are empty. The corresponding density is shown in Fig. 5(b), in which the red and black dotted lines indicate critical values  $i \approx 17$  and  $i \approx 42$ , respectively.

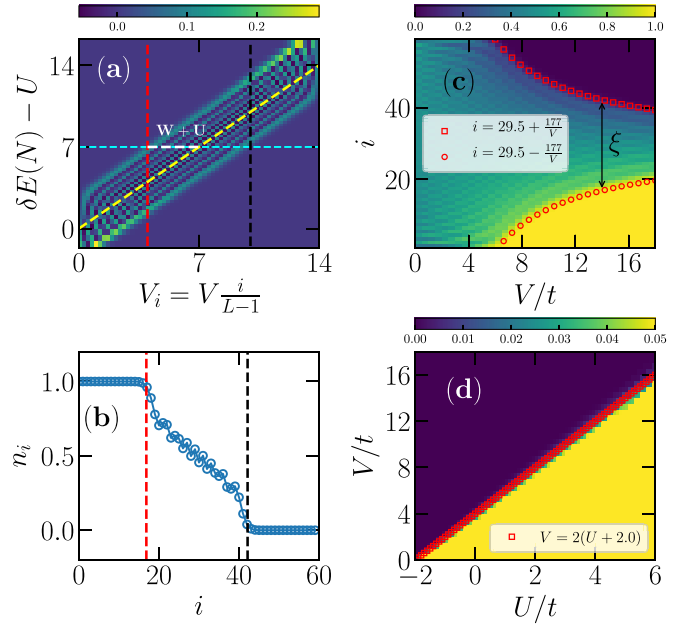


FIG. 5. (a) The distribution of  $\delta n_i(N)$  for  $U/t = 1$  and  $V/t = 14$ . (b)  $n_i$  for  $U/t = 1$  and  $V/t = 14$ . (c) Scan of  $n_i$  as a function of  $V/t$  for  $U/t = 1$ . (d) The  $n_{i=L-1}$  for different  $U/t$  and  $V/t$ . Here we use the open boundary condition and set  $L = 60$ . The red and black lines in (a) correspond to those in (b). In (b)–(d), the filling factor is  $\rho = 0.5$ . The abscissa in (b) and the ordinate in (c) indicate the site  $i$ . The color represents the value of  $\delta n_i(N)$  in (a) and  $n_i$  in (c), (d). To indicate transition points clearly, we control the range of the color bar from 0.0 to 0.05 in (d).

Then we consider more general cases for different  $V$ . Based on the distribution in Fig. 5(a) and the analysis in Fig. 3, one can obtain that the site  $i$  is fully occupied when it satisfies  $E_{\text{center}} - (W+U) \geq V \frac{i}{L-1}$  and it is empty when it satisfies  $E_{\text{center}} + (W+U) \leq V \frac{i}{L-1}$ , namely

$$n_i = \begin{cases} 1, & i \leq \frac{E_{\text{center}} - U - W}{V}(L-1), \\ 0, & i \geq \frac{E_{\text{center}} + U + W}{V}(L-1). \end{cases} \quad (5)$$

For half-filling,  $E_{\text{center}} \approx V/2$  as shown in Fig. 5(a), thus we obtain

$$n_i = \begin{cases} 1, & i \leq \left(\frac{1}{2} - \frac{U+W}{V}\right)(L-1), \\ 0, & i \geq \left(\frac{1}{2} + \frac{U+W}{V}\right)(L-1). \end{cases} \quad (6)$$

From Eq. (6), one can obtain that the lengthscale of the ground state is  $\xi = 2(U+W)(L-1)/V$ , indicating the difference between two critical values  $\left(\frac{1}{2} - \frac{U+W}{V}\right)(L-1)$  and  $\left(\frac{1}{2} + \frac{U+W}{V}\right)(L-1)$ . In Fig. 5(c), we show the scan of  $n_i$  for  $U/t = 1.0$  and different  $V/t$ , in which Eq. (6) is well-confirmed. The width between different markers indicates the  $V$ -dependent lengthscale  $\xi = \xi(V)$ . It is larger than the system size  $\xi > L$  for  $V/t < 6.0$ , whereas it is smaller than the system size  $\xi < L$  for  $V/t > 6.0$ . The ground-state energy in Appendix C shows that this transition is a continuous phase transition. By varying  $U/t$ , we also study the effect of the interaction on the transition point. Intuitively,  $n_{i=0} = 1$  or  $n_{i=L-1} = 0$  as  $V$  increases, and the localization transition

occurs as shown in Fig. 5(c), thus the transition point should satisfy  $(\frac{1}{2} - \frac{U+W}{V})(L-1) = 0$  or  $(\frac{1}{2} + \frac{U+W}{V})(L-1) = L-1$ , which derives

$$V_c = 2(U + W). \quad (7)$$

In Fig. 5(d), we show  $n_{i=L-1}$  for different  $U/t$  and  $V/t$ , which indicates that the transition points are well captured by Eq. (7). It is worth pointing out that the localization transition point of the many-body system for  $U/t = 0$  is at  $V_c/t = 4$ , whereas the single-particle transition point in the ground state is at  $V_c/t = 0$  as shown in Fig. 2(a). This is due to the fact that the eigenstate of the many-body system is the superposition of that of the single particle, which causes the transition point to be determined by the single-particle state with the largest expansion. Furthermore, we find that the system is in the localization region for  $U/t < -2.0$  with any  $V/t$ . It can be understood that the energy provided by the attractive interaction for  $U/t < -2.0$  is greater than that provided by the hopping term, resulting in the halt of extension.

### C. Dynamical localization of different domain-wall initial states

Now let us study the dynamical localization transition of the many-body system. We first consider the initial state  $|100\dots 000\rangle$ , and then we add bosons one by one in order until all sites are filled,  $|111\dots 111\rangle$ . We define that, at time  $\mathcal{T}$ , the density distribution is  $n_i(N, \mathcal{T})$ , where  $i$  is the site and  $N$  denotes the number of bosons in the initial state. By calculating the density difference  $\delta n_i(N, \mathcal{T}) = n_i(N+1, \mathcal{T}) - n_i(N, \mathcal{T})$ , we can obtain the distribution of the added boson. In Fig. 6(a), we show the distribution of  $\delta n_i(N, \mathcal{T})$  for  $U/t = 1$ ,  $V/t = 24$ , and  $\mathcal{T}/t = 10000$ , in which the ordinate  $V_j$  is the local potential energy of the added boson at the site  $j$ . The distribution of  $\delta n_i(N, \mathcal{T})$  has a center at  $V_i \approx V_j$  (the yellow dotted line), which is similar to  $|\psi_i(j, \mathcal{T})|^2$  in Fig. 3(c). The half-width  $2(W+U)$  (the white dotted line) is extracted from Fig. 5(a), which is confirmed by  $\delta n_i(N, \mathcal{T})$  in Fig. 6(a). We set the initial state as  $|111\dots 000\rangle$  with half-filling, i.e., the distributions with energy  $V_j \leq V/2t = 12$  are filled (the region below the cyan dotted line). Due to the number of bosons  $N$  being fixed for half-filling, we abbreviate  $n_i(N, \mathcal{T})$  to  $n_i(\mathcal{T})$ . By analogy with Figs. 3(c) and 3(d), we can obtain that the site  $i$  is fully occupied when it satisfies  $V/2 - 2(W+U) \geq V \frac{i}{L-1}$ , and it is empty when it satisfies  $V/2 + 2(W+U) \leq V \frac{i}{L-1}$ , namely

$$n_i(\mathcal{T}) = \begin{cases} 1, & i \leq [\frac{1}{2} - \frac{2(U+W)}{V}](L-1), \\ 0, & i \geq [\frac{1}{2} + \frac{2(U+W)}{V}](L-1). \end{cases} \quad (8)$$

Thus the dynamical lengthscale of  $|111\dots 000\rangle$  is  $\xi = 4(U+W)(L-1)/V$ . The typical density for  $U/t = 1$ ,  $V/t = 24$ ,  $L = 18$ , and  $\mathcal{T}/t = 10000$  is shown in Fig. 6(b), in which the red (black) dotted line indicates  $i = 4.25$  ( $i = 12.75$ ), corresponding to that at  $V_i/t = 6$  ( $V_i/t = 18$ ) in Fig. 6(a). We also show  $n_i(\mathcal{T})$  for different  $V/t$  in Fig. 6(c), where Eq. (8) gives a nice indication. Similar to the ground state,  $n_{i=0}(\mathcal{T}) = 1$  or  $n_{i=L-1}(\mathcal{T}) = 0$  indicates that the transition occurs. Thus we can obtain that the dynamical transition point is at

$$V_d = 4(U + W). \quad (9)$$

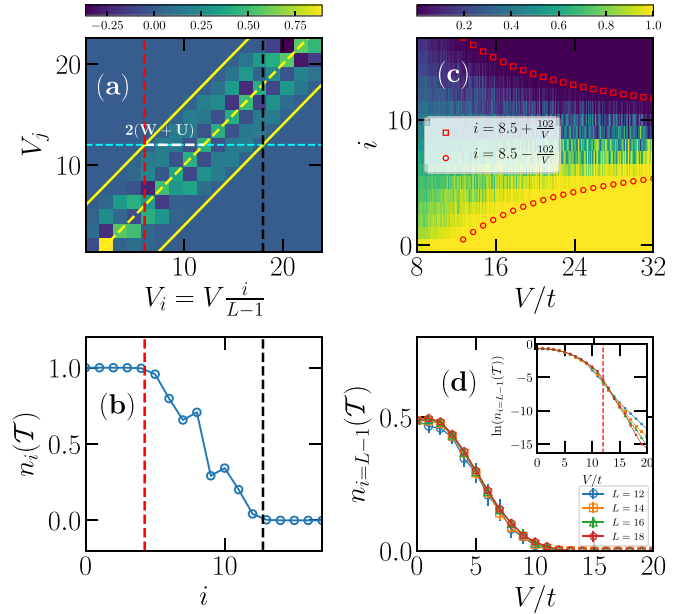


FIG. 6. (a) The distribution of  $\delta n_i(N, \mathcal{T})$  for  $V/t = 24$ . (b)  $n_i(\mathcal{T})$  for  $V/t = 24$ . (c) Scan of  $n_i(\mathcal{T})$  as a function of  $V/t$ . (d)  $n_{i=L-1}(\mathcal{T})$  as a function of  $V/t$ . Here we use the open boundary condition and set  $L = 18$ ,  $U/t = 1$ , and time  $\mathcal{T}/t = 10000$ . In (a), the yellow dotted line and yellow solid lines indicate the center and edges of  $\delta n_i(N, \mathcal{T}) \neq 0$ , respectively. In (b)–(d), the filling factor  $\rho = 0.5$ . The color represents the value of  $\delta n_i(N, \mathcal{T})$  in (a) and  $n_i(\mathcal{T})$  in (c). In (d), the inset shows  $\ln(n_{i=L-1}(\mathcal{T}))$  and error bars are from 10 000 time samples.

In Fig. 6(d), we fix the object as  $i = L-1$  and study  $n_{i=L-1}(\mathcal{T})$  for  $U/t = 1$  and different  $V$ .  $n_{i=L-1}(\mathcal{T})$  decreases gradually as  $V$  increases, and  $n_{i=L-1}(\mathcal{T}) \approx 0$  for about  $V/t > 12$ . An analysis of the size effect can be found in the inset, where the curves for different  $L$  intersect at  $V_d/t \approx 12$ .

To further study the effect of the interaction, we fix the initial state  $|111\dots 000\rangle$  and vary the interaction to seek transition points. Intuitively, the critical amplitude should increase with the repulsive interaction from Eq. (9). However, interestingly, we find that the diffusion of bosons is suppressed when the repulsive interaction is strong, as demonstrated in Fig. 7(a). Typical examples for  $U/t > 0$  are shown in Fig. 7(b), in which the interaction first promotes the extension, and then suppresses it as  $U/t$  increases. To clarify the competition between the interaction and the linear potential, we show a whole phase diagram in Fig. 7(c), in which the parameters  $(V, U)$  and  $(-V, -U)$  have a nice symmetry [the details are given in Fig. 7(d)]. This is consistent with Ref. [67], and by this symmetry one may get that another critical point of the dynamical transition is at

$$V_d = 4(U - W), \quad (10)$$

which is evidenced in Fig. 7(c). In particular, we notice that the system is in the localization region for about  $|U/t| > 4.0$  and any  $V/t$ . A simple understanding is that the maximum energy that the hopping term can provide in the dynamical case is  $4t$ , thus the extension is completely suppressed for  $U/t < -4.0$ . By the symmetry of the parameters  $(V, U)$  and

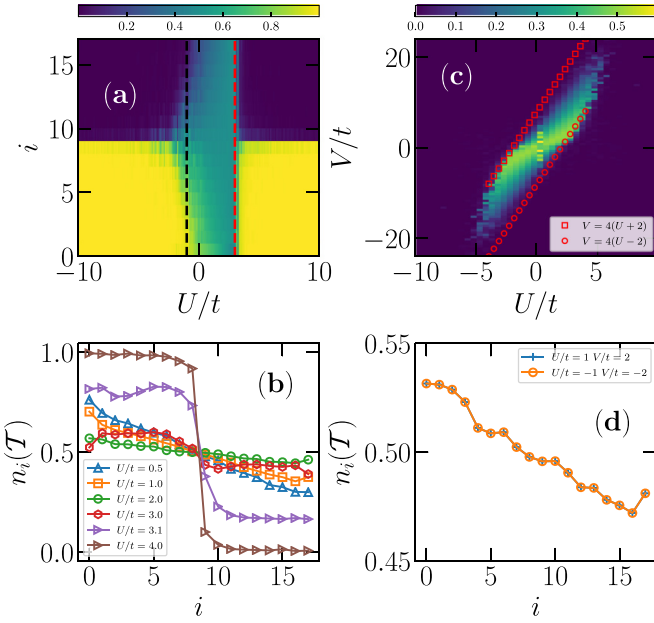


FIG. 7. (a) Scan of  $n_i(\mathcal{T})$  for different  $U$ 's and typical examples are shown in (b). (c)  $n_i(\mathcal{T})$  for a fixed site  $i = L - 1$  and different  $U$ 's and  $V$ 's. (d)  $n_i(\mathcal{T})$  for  $(U, V)$  and  $(-U, -V)$ . Here we use the open boundary condition and set  $L = 18$ ,  $\mathcal{T}/t = 10000$ . In (a),  $V/t = 4.0$  and the black (red) dotted line marks  $U/t = -1.0$  ( $U/t = 3.0$ ). The color in (a) and (c) represents  $n_i(\mathcal{T})$  and  $n_{i=L-1}(\mathcal{T})$ , respectively.

$(-V, -U)$ , one can obtain that  $|111 \dots 000\rangle$  exhibits dynamical localization for  $|U/t| > 4.0$ .

In addition to  $|111 \dots 000\rangle$ , we also study the dynamical localization transition of  $|000 \dots 111\rangle$ . To obtain the distribution of  $\delta n_i(N, \mathcal{T})$ , we fill the bosons in reverse order, i.e., starting from  $|000 \dots 001\rangle$  to  $|111 \dots 111\rangle$ . In Fig. 8(a), we show the distribution of  $\delta n_i(N, \mathcal{T})$  for  $V/t = 8$ , which is similar to that in Fig. 6(a), but the half-width changes to  $2(W - U)$ . Here, the sign of the interaction changes in order to keep the conservation of energy [48,68]. In Fig. 8(b), we show the scan of  $n_i(\mathcal{T})$  for  $U/t = 1$  and different  $V$ , where Eqs. (8) and (9) still work with the sign change of the interaction, and the transition point is at  $V_d/t = 4(-U + W)/t = 4$ . Compared with  $|111 \dots 000\rangle$  and  $|000 \dots 111\rangle$ , it might be more interesting to study a general domain-wall initial state, e.g.,  $|00 \dots 111 \dots 000\rangle$ . We choose a general domain-wall initial state as an example in which we set bosons local between  $i = 4$  and  $12$ . In Fig. 8(c), we show  $n_i(\mathcal{T})$  for different initial states, in which the two wings of  $n_i(\mathcal{T})$  of  $|00 \dots 111 \dots 000\rangle$  can be obtained approximately by shifting that of  $|111 \dots 000\rangle$  and  $|000 \dots 111\rangle$ . This is in agreement with Ref. [48], and the slight difference comes from the boundary effect. In Fig. 8(d), we show the scan of  $n_i(\mathcal{T})$  of  $|00 \dots 111 \dots 000\rangle$  for different  $V$ . The red and black markers are obtained by shifting those in Figs. 6(c) and 8(b), respectively. Obviously, the markers identify the critical positions well.

Our starting point of the dynamics of domain-wall states is Ref. [48], thus it is necessary to show the difference between our paper and Ref. [48]. First, we adopt a weak linear potential to study the localization and show more details of the

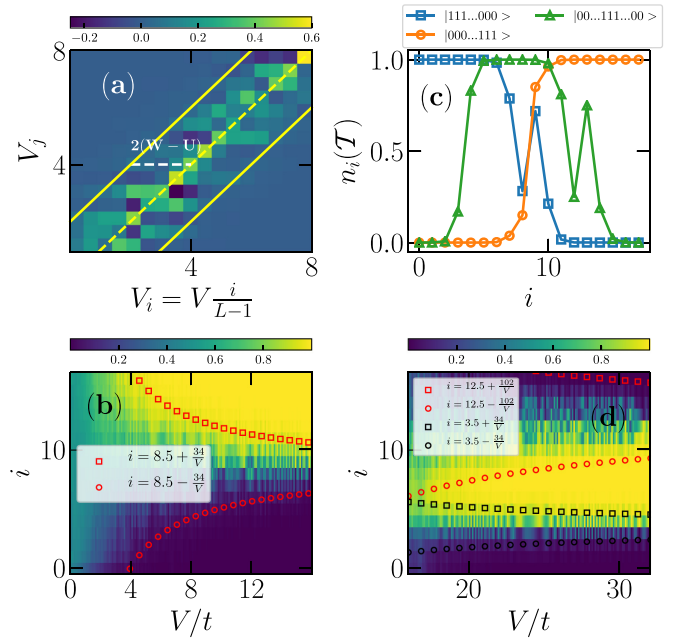


FIG. 8. (a) The distribution of  $\delta n_i(N, \mathcal{T})$  for  $V/t = 8$ . (b) Scan of  $n_i(\mathcal{T})$  as a function of  $V/t$  for  $|000 \dots 111\rangle$ . (c)  $n_i(\mathcal{T})$  for different domain-wall initial states and  $V/t = 35$ . (d) Scan of  $n_i(\mathcal{T})$  as a function of  $V/t$  for  $|00 \dots 111 \dots 000\rangle$ . Here we use the open boundary condition and set  $L = 18$ ,  $U/t = 1$ , and time  $\mathcal{T}/t = 10000$ . In (b)–(d), the filling factor  $\rho = 0.5$ . The color represents the value of  $\delta n_i(N, \mathcal{T})$  in (a) and  $n_i(\mathcal{T})$  in (c), (d).

transition. Second, in our paper, we obtain the specific formula of the lengthscale  $\xi = 4(U + W)(L - 1)/V$  and clarify how parameters of the linear potential  $V$  and the interaction  $U$  affect  $\xi$ . In particular, we find that the strong repulsive interaction suppresses  $\xi$  and promotes dynamical localization. Third, we also consider the nonlinear potential case in Appendix D to show that our analysis is general for dynamics of domain-wall states in systems with ordered potentials.

Then we proceed to investigate the imbalance  $\mathcal{I} = (n_\bullet - n_\circ)/(n_\bullet + n_\circ)$ , where  $\bullet$  ( $\circ$ ) marks the occupied (not occupied) sites in the initial state [8,20]. Here, we still fix  $|111 \dots 000\rangle$  as an initial state. In Fig. 9(a), we show  $\mathcal{I}$  between  $\mathcal{T}/t = 10250$  and  $10550$ . Time  $\mathcal{T}/t \approx 10^4$  is long enough to characterize the long-time behavior [48]. The parameters of the interaction and the potential are  $U/t = 1$  and  $V/t = 12$ , which is the critical point indicated by Eq. (9). Interestingly,  $\mathcal{I}$  has an approximate periodic oscillation, and the period is  $\Delta\mathcal{T}/t \approx 11.6$ . The corresponding densities as a function of  $\mathcal{T}$  are shown in Fig. 9(b), where the density oscillates periodically, dubbed many-body Bloch oscillations [44]. When the oscillation amplitude is maximum, the bosons are distributed in the whole chain. The typical densities  $n_i(\mathcal{T})$  of maximum and minimum oscillation amplitudes are shown in Fig. 9(c). When  $\mathcal{T}/t = 10399$ ,  $n_i(\mathcal{T}) \approx 1 - i/(L - 1)$  is approximately linearly distributed. This is in agreement with Ref. [48], in which densities are not uniformly distributed. Generally, the imbalance  $\mathcal{I} = 0.0$  or not is an important indicator for the transition [8]. However, the imbalance of the distribution  $n_i(\mathcal{T}) = 1 - i/(L - 1)$  should be  $\mathcal{I} \approx 0.5$  instead of  $\mathcal{I} \approx 0.0$ , as shown in Fig. 9(a). This means that the transition point

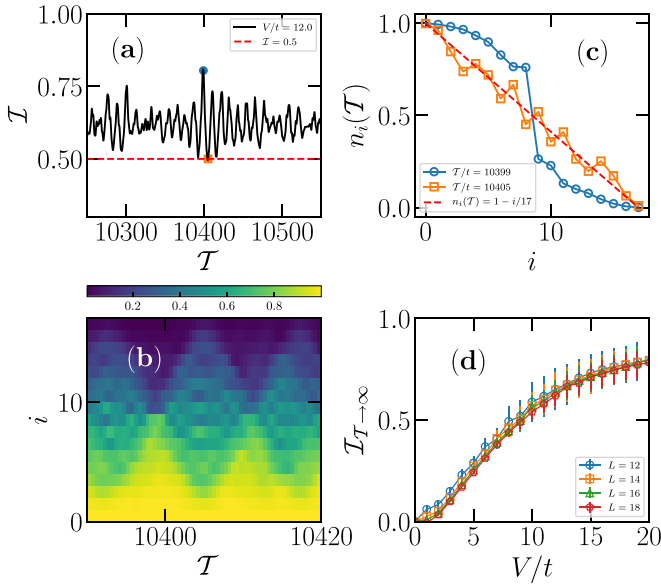


FIG. 9. Imbalance  $\mathcal{I}$  for the long-time evolution in (a). The scan of density  $n_i(\mathcal{T})$  for  $10390 < \mathcal{T}/t < 10420$  in (b).  $n_i(\mathcal{T})$  for  $\mathcal{T}/t = 10399$  and  $10405$  in (c), which corresponds to the points of the same color in (a). Long-time imbalance  $\mathcal{I}_{\mathcal{T} \rightarrow \infty}$  for different sizes in (d). Here we use the open boundary condition and set  $\rho = 0.5$ ,  $U/t = 1$ . In (a)–(c),  $L = 18$ ,  $V/t = 12.0$ . The red dashed lines in (a),(c) represent ideal  $\mathcal{I}$  and  $n_i(\mathcal{T})$ . The error bars are from 10 000 time samples in (d).

indicated by the imbalance  $\mathcal{I} \approx 0.0$  is different from Eq. (9). In Fig. 9(d), we show the long-time imbalance for different  $V$ , in which the transition point indicated by  $\mathcal{I} \approx 0.0$  is much smaller than that indicated by  $n_{i=L-1}(\mathcal{T})$  in Fig. 6(d). This can be attributed to the inability of the domain-wall configuration to evolve into a uniform configuration [31].

## V. CONCLUSION

To summarize, we have studied hard-core bosons in a lattice chain with a linear potential. In the present work, we have carefully studied both the single-particle and the many-body cases.

In the single-particle case, we find that the dynamical localization transition point is different from the static localization transition point, indicating the presence of an intermediate phase. In this intermediate phase, the eigenstates behave as static localization, but dynamic wave functions after quenching are extended. By analyzing the distribution of eigenstates, we have clarified the reason for the occurrence of this intermediate phase.

In the many-body case, we find a many-body intermediate phase by comparing the static critical point with the dynamical critical point. This many-body intermediate phase is analogous to the single-particle intermediate phase, but different from the many-body intermediate phase with nonergodic delocalized states [22–25]. In addition to the many-body intermediate phase, we also study the ground-state transition by DMRG. Interestingly, we find that the distribution of  $\delta n_i(N)$  of the many-body state is similar to  $|c_i^n|^2$  of the single-particle state, and they can both be described by the

conservation of energy. By numerical verification, we find that the static transition occurs at  $V_c \approx 2(U + W)$  for half-filling in the ground state. Then we turn to study the dynamical transition for different initial states. For the typical domain-wall state  $|111 \dots 000\rangle$ , its dynamical transition points are at  $V_d \approx 4(U + W)$  and  $V_d \approx 4(U - W)$ . For another typical domain-wall state  $|000 \dots 111\rangle$ , its dynamical transition points are at  $V_d \approx 4(-U + W)$  and  $V_d \approx 4(-U - W)$ . The critical points of other domain-wall states can be obtained by shifting those of the above two states. Finally, we study the imbalance  $\mathcal{I}$  to reveal how domain-wall states retain local information after quenching.

## ACKNOWLEDGMENTS

This work was supported by “Pioneer” and “Leading Goose” R&D Program of Zhejiang (2022SDXHXDX0005), the Key R&D Program of Zhejiang Province (2021C01002), and the foundation from Westlake University. We thank Westlake University HPC Center for computation support. The DMRG calculations were performed using the ALPS libraries.

## APPENDIX A: EIGENSTATES AND WAVE FUNCTIONS FOR DIFFERENT PHASES

In Fig. 10, we show the typical eigenstates  $|c_i^n|^2$  and wave functions  $|\psi_i(j, \mathcal{T})|^2$  for extended, intermediate, localized phases. In the extended phase in (a),(b), the eigenstate and wave function populate the whole chain. In the intermediate phase in (c),(d), the eigenstate is bounded but the wave function still populates the whole chain. In the localized phase in (e),(f), they both localized in the chain.

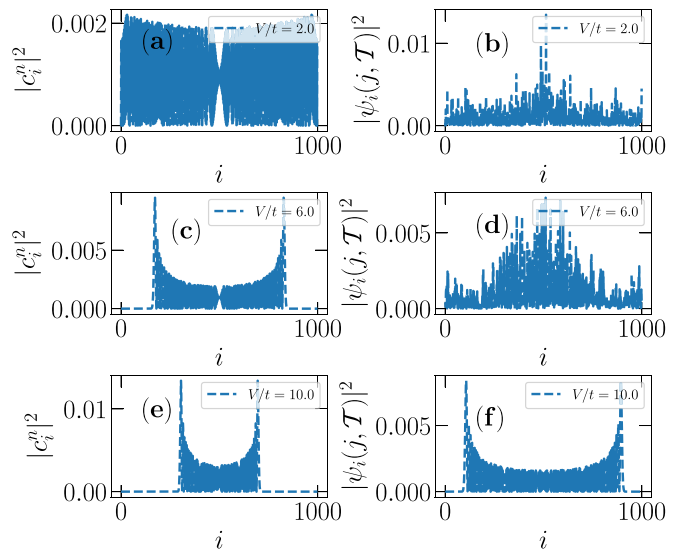


FIG. 10. Left panels: Eigenstates  $|c_i^n|^2$  with  $n = L/2$  for different  $V/t$ . Right panels: wave functions  $|\psi_i(j, \mathcal{T})|^2$  with  $j = L/2$  and  $\mathcal{T} = 10000.5\mathcal{T}_b$  for different  $V/t$ .  $L = 1000$ . Parts (c) and (d) show the typical eigenstate and wave function in the intermediate phase, respectively.



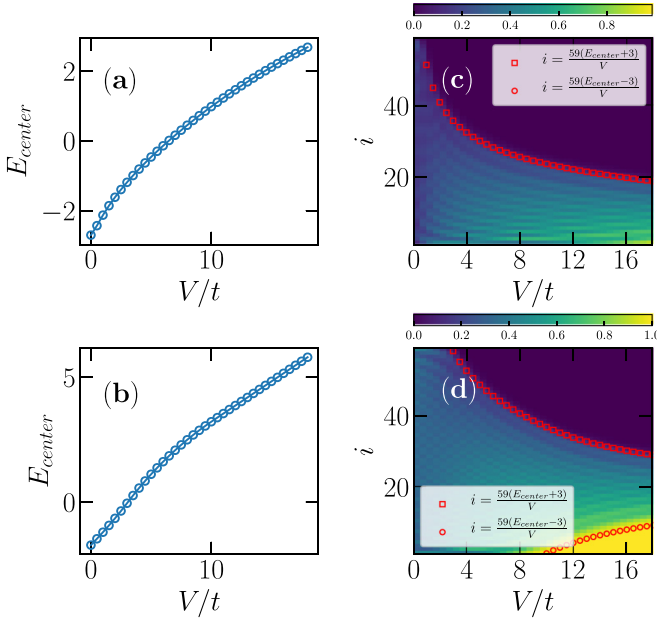


FIG. 11. (a)  $E_{\text{center}} = \delta E(N) - U$  as a function of  $V/t$  for  $\rho = 1/6$ . (b) Scan of  $n_i$  as a function of  $V/t$  for  $\rho = 1/6$ . (c)  $E_{\text{center}} = \delta E(N) - U$  as a function of  $V/t$  for  $\rho = 1/3$ . (d) Scan of  $n_i$  as a function of  $V/t$  for  $\rho = 1/3$ .  $L = 60$ ,  $U/t = 1.0$ .

### APPENDIX B: EFFECT OF THE FILLING FACTOR

In the main text, we fixed the filling factor as  $\rho = 0.5$ . Here we choose different filling factors to study the effect on  $\xi$ . In Fig. 5(a), the distribution of  $\delta n_i(N)$  has a center at  $E_{\text{center}} = \delta E(N) - U$  with a half-width  $(W + U)/t = 3$ . Obviously, the adjustment of the filling factor alters the central energy  $E_{\text{center}}$ . In Figs. 11(a) and 11(c), we show  $E_{\text{center}}$  as a function of  $V/t$  for  $\rho = 1/6$  and  $1/3$ , respectively. Similar to the analysis in the main text, one can obtain that the site  $i$  is fully occupied when it satisfies  $E_{\text{center}} - (W + U) \geq V \frac{i}{L-1}$ , and it is empty when it satisfies  $E_{\text{center}} + (W + U) \leq V \frac{i}{L-1}$ , namely

$$n_i = \begin{cases} 1, & i \leq \frac{(E_{\text{center}} - U - W)(L-1)}{V}, \\ 0, & i \geq \frac{(E_{\text{center}} + U + W)(L-1)}{V}. \end{cases} \quad (\text{B1})$$

This is well confirmed in Figs. 12(c) and 12(d). The length-scale of the ground state is still  $\xi = 2(U + W)(L - 1)/V$ , thus one can conclude that the filling factor does not affect  $\xi$ .

### APPENDIX C: GROUND-STATE ENERGY AND IPR IN THE GROUND STATE

In Fig. 12(a), we show the ground-state energies  $E_0$  for different  $V/t$ , and different derivatives of  $E_0$  are shown in (b)–(d).  $E_0$  and its first derivative are continuous functions of  $V/t$ , whereas the second and third derivatives are not. This demonstrates that the transition in Fig. 5(c) is a continuous phase transition. Moreover, one can obtain that the transition point is at  $V/t \approx 6.0$  from Figs. 12(c) and 12(d).

In addition to the lengthscale  $\xi$  in the main text, we also use IPR to distinguish the localization in the ground state. In

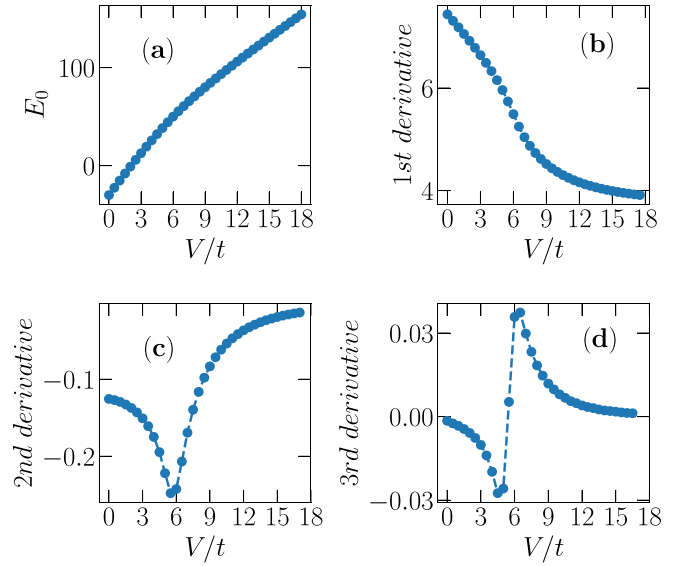


FIG. 12. (a) The ground-state energies  $E_0$  for different  $V/t$ . Parts (b), (c), and (d) show the first, second, and third derivatives of  $E_0$ , respectively.  $L = 60$ ,  $N = 30$ , and  $U/t = 1.0$ .

the many-body case, the many-body wave function expands as the Hilbert space increases whether it is a delocalized state or a localized state, thus IPR decreases as  $L$  increases both for the delocalized state and the localized state as shown in Fig. 13(a). For perfectly delocalized states,  $\text{IPR} \propto 1/\mathcal{N}$ , where  $\mathcal{N}$  is the dimension of the Hilbert space. For localized states, the proportion does not hold. Thus one may use  $\text{IPR} * \mathcal{N}$  to seek the transition point. In Fig. 13(b), we show  $\text{IPR} * \mathcal{N}$  as a function of  $V/t$  for different  $L$ 's, in which  $\text{IPR} * \mathcal{N}$  for different sizes  $L$ 's is small and does not depend on  $L$  significantly in the delocalized phase, whereas  $\text{IPR} * \mathcal{N}$  increases with  $L$  rapidly in the localized phase. The transition point  $V/t \approx 6.0$  is the same as that indicated by  $\xi$ .

### APPENDIX D: NONLINEAR POTENTIAL

In the main text, we showed the results of a system with a linear potential. Here we consider the nonlinear case with a

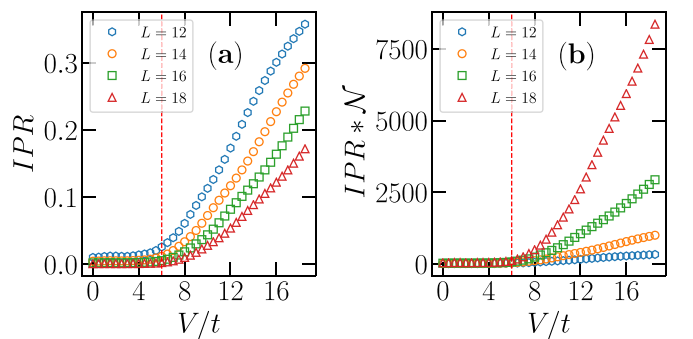


FIG. 13. (a) IPR as a function of  $V/t$  for different  $L$ 's in the ground state. (b)  $\text{IPR} * \mathcal{N}$  as a function of  $V/t$  for different  $L$ 's in the ground state. The filling factor  $\rho = 0.5$ ,  $U/t = 1.0$ . Here we use the open boundary condition. The red dotted lines indicate  $V/t = 6.0$  in (a) and (b).

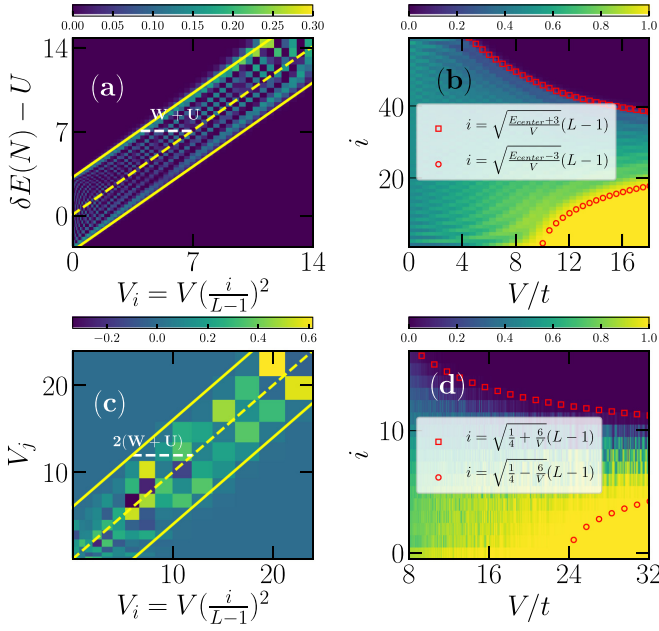


FIG. 14. (a) The distribution of  $\delta n_i(N)$  for  $V/t = 14$ . (b) The scan of  $n_i$  for different  $V/t$ . (c) The distribution of  $\delta n_i(N, T)$  for  $V/t = 24$  and  $T/t = 10000$ . (d)  $n_i(T)$  for  $V/t = 24$  and  $T/t = 10000$ . Here we use the open boundary condition and set  $\rho = N/L = 0.5$  and  $U/t = 1$ .  $L = 60$  in (a),(b) and  $L = 18$  in (c),(d).

harmonic potential  $V_i = V(\frac{i}{L-1})^2$ . In Fig. 14(a), we show the distribution of  $\delta n_i(N)$ , which has a center at  $V_i = \delta E(N) - U$  with a half-width  $(W + U)/t = 3$ . It is similar to Fig. 5 due to the fact that the distribution of  $\delta n_i(N)$  is based on energy

conservation, independent of the potential form. In Fig. 14(b), we show the scan of  $n_i$  for different  $V/t$ . Based on the distribution in Fig. 14(a), one can obtain that the site  $i$  is fully occupied when it satisfies  $E_{\text{center}} - (W + U) \geq V(\frac{i}{L-1})^2$ , and it is empty when it satisfies  $E_{\text{center}} + (W + U) \leq V(\frac{i}{L-1})^2$ , namely

$$n_i = \begin{cases} 1, & i \leq \sqrt{\frac{E_{\text{center}} - U - W}{V}}(L - 1), \\ 0, & i \geq \sqrt{\frac{E_{\text{center}} + U + W}{V}}(L - 1), \end{cases} \quad (\text{D1})$$

which is confirmed in Fig. 14(b). Thus the lengthscale is  $(\sqrt{\frac{E_{\text{center}} + U + W}{V}} - \sqrt{\frac{E_{\text{center}} - U - W}{V}})(L - 1)$ . Then we study the dynamical localization of the domain-wall initial state  $|111 \dots 000\rangle$  with half-filling. In Fig. 14(c), we show the distribution of  $\delta n_i(N, T)$  for  $T/t = 10000$ . It has a center at  $V_i \approx V_j$  with a half-width  $2(W + U)/t = 6$ . Based on it, one can obtain that the site  $i$  is fully occupied when it satisfies  $\frac{V}{4} - 2(W + U) \geq V(\frac{i}{L-1})^2$ , and it is empty when it satisfies  $\frac{V}{4} + 2(W + U) \leq V(\frac{i}{L-1})^2$ , where the center energy  $\frac{V}{4}$  is from  $V(\frac{i}{L-1})^2$  due to half-filling  $\frac{i}{L-1} \approx \frac{1}{2}$ . Thus we obtain

$$n_i = \begin{cases} 1, & i \leq \sqrt{\frac{1}{4} - \frac{2(U+W)}{V}}(L - 1), \\ 0, & i \geq \sqrt{\frac{1}{4} + \frac{2(U+W)}{V}}(L - 1), \end{cases} \quad (\text{D2})$$

with the dynamical lengthscale  $(\sqrt{\frac{1}{4} + \frac{2(U+W)}{V}} - \sqrt{\frac{1}{4} - \frac{2(U+W)}{V}})(L - 1)$ . We verify it in Fig. 14(d), where Eq. (D2) gives a nice indication.

- 
- [1] D. M. Basko, I. L. Aleiner, and B. L. Altshuler, *Ann. Phys.* **321**, 1126 (2006).
- [2] A. Pal and D. A. Huse, *Phys. Rev. B* **82**, 174411 (2010).
- [3] R. Nandkishore and D. A. Huse, *Annu. Rev. Condens. Matter Phys.* **6**, 15 (2015).
- [4] F. Alet and N. Laflorencie, *C. R. Phys.* **19**, 498 (2018).
- [5] J. H. Bardarson, F. Pollmann, and J. E. Moore, *Phys. Rev. Lett.* **109**, 017202 (2012).
- [6] V. Khemani, D. N. Sheng, and D. A. Huse, *Phys. Rev. Lett.* **119**, 075702 (2017).
- [7] D. A. Abanin and Z. Papić, *Ann. Phys.* **529**, 1700169 (2017).
- [8] M. Schreiber, S. S. Hodgman, P. Bordia, H. P. Lüschen, M. H. Fischer, R. Vosk, E. Altman, U. Schneider, and I. Bloch, *Science* **349**, 842 (2015).
- [9] A. Chakraborty, P. Gorantla, and R. Sensarma, *Phys. Rev. B* **102**, 224306 (2020).
- [10] R. Lewis-Swan, A. Safavi-Naini, A. Kaufman, and A. Rey, *Nat. Rev. Phys.* **1**, 627 (2019).
- [11] M. Serbyn and J. E. Moore, *Phys. Rev. B* **93**, 041424(R) (2016).
- [12] D. J. Luitz, N. Laflorencie, and F. Alet, *Phys. Rev. B* **91**, 081103(R) (2015).
- [13] V. Khemani, A. Lazarides, R. Moessner, and S. L. Sondhi, *Phys. Rev. Lett.* **116**, 250401 (2016).
- [14] J. Zhang, P. Hess, A. Kyprianidis, P. Becker, A. Lee, J. Smith, G. Pagano, I.-D. Potirniche, A. C. Potter, A. Vishwanath *et al.*, *Nature (London)* **543**, 217 (2017).
- [15] D. V. Else, B. Bauer, and C. Nayak, *Phys. Rev. Lett.* **117**, 090402 (2016).
- [16] N. Y. Yao, A. C. Potter, I.-D. Potirniche, and A. Vishwanath, *Phys. Rev. Lett.* **118**, 030401 (2017).
- [17] W. W. Ho, S. Choi, M. D. Lukin, and D. A. Abanin, *Phys. Rev. Lett.* **119**, 010602 (2017).
- [18] A. Kshetrimayum, J. Eisert, and D. M. Kennes, *Phys. Rev. B* **102**, 195116 (2020).
- [19] W. De Roeck, F. Huveneers, M. Müller, and M. Schiulaz, *Phys. Rev. B* **93**, 014203 (2016).
- [20] X. Wei, C. Cheng, G. Xianlong, and R. Mondaini, *Phys. Rev. B* **99**, 165137 (2019).
- [21] T. Kohlert, S. Scherg, X. Li, H. P. Lüschen, S. Das Sarma, I. Bloch, and M. Aidelsburger, *Phys. Rev. Lett.* **122**, 170403 (2019).
- [22] X.-P. Li, S. Ganeshan, J. H. Pixley, and S. Das Sarma, *Phys. Rev. Lett.* **115**, 186601 (2015).
- [23] R. Modak and S. Mukerjee, *Phys. Rev. Lett.* **115**, 230401 (2015).
- [24] Y.-T. Hsu, X. Li, D.-L. Deng, and S. Das Sarma, *Phys. Rev. Lett.* **121**, 245701 (2018).

- [25] E. J. Torres-Herrera and L. F. Santos, *Ann. Phys.* **529**, 1600284 (2017).
- [26] J. Šuntajs, J. Bonča, T. c. v. Prosen, and L. Vidmar, *Phys. Rev. E* **102**, 062144 (2020).
- [27] R. K. Panda, A. Scardicchio, M. Schulz, S. R. Taylor, and M. Žnidarič, *Europhys. Lett.* **128**, 67003 (2020).
- [28] D. A. Abanin, J. H. Bardarson, G. De Tomasi, S. Gopalakrishnan, V. Khemani, S. A. Parameswaran, F. Pollmann, A. C. Potter, M. Serbyn, and R. Vasseur, *Ann. Phys.* **427**, 168415 (2021).
- [29] R. Mondaini and Z. Cai, *Phys. Rev. B* **96**, 035153 (2017).
- [30] M. Schulz, C. A. Hooley, R. Moessner, and F. Pollmann, *Phys. Rev. Lett.* **122**, 040606 (2019).
- [31] E. van Nieuwenburg, Y. Baum, and G. Refael, *Proc. Natl. Acad. Sci. (USA)* **116**, 9269 (2019).
- [32] G. H. Wannier, *Rev. Mod. Phys.* **34**, 645 (1962).
- [33] L.-N. Wu and A. Eckardt, *Phys. Rev. Lett.* **123**, 030602 (2019).
- [34] R. Yao, T. Chanda, and J. Zakrzewski, *Phys. Rev. B* **104**, 014201 (2021).
- [35] T. Chanda, R. Yao, and J. Zakrzewski, *Phys. Rev. Res.* **2**, 032039(R) (2020).
- [36] Z.-H. Sun, J. Cui, and H. Fan, *Phys. Rev. Res.* **2**, 013163 (2020).
- [37] S. R. Taylor, M. Schulz, F. Pollmann, and R. Moessner, *Phys. Rev. B* **102**, 054206 (2020).
- [38] Y.-Y. Wang, Z.-H. Sun, and H. Fan, *Phys. Rev. B* **104**, 205122 (2021).
- [39] W. Morong, F. Liu, P. Becker, K. S. Collins, L. Feng, A. Kyprianidis, G. Pagano, T. You, A. V. Gorshkov, and C. Monroe, *Nature (London)* **599**, 393 (2021).
- [40] X.-Y. Guo, Z.-Y. Ge, H. Li, Z. Wang, Y.-R. Zhang, P. Song, Z. Xiang, X. Song, Y. Jin, L. Lu *et al.*, *npj Quantum Inf.* **7**, 51 (2021).
- [41] Q. Guo, C. Cheng, H. Li, S. Xu, P. Zhang, Z. Wang, C. Song, W. Liu, W. Ren, H. Dong, R. Mondaini, and H. Wang, *Phys. Rev. Lett.* **127**, 240502 (2021).
- [42] T. Kohlert, S. Scherg, P. Sala, F. Pollmann, B. H. Madhusudhana, I. Bloch, and M. Aidelsburger, [arXiv:2106.15586](https://arxiv.org/abs/2106.15586) [cond-mat.quant-gas].
- [43] S. Scherg, T. Kohlert, P. Sala, F. Pollmann, B. H. Madhusudhana, I. Bloch, and M. Aidelsburger, *Nat. Commun.* **12**, 4490 (2021).
- [44] P. Ribeiro, A. Lazarides, and M. Haque, *Phys. Rev. Lett.* **124**, 110603 (2020).
- [45] L. D'Alessio, Y. Kafri, A. Polkovnikov, and M. Rigol, *Adv. Phys.* **65**, 239 (2016).
- [46] R. Mondaini, K. R. Fratus, M. Srednicki, and M. Rigol, *Phys. Rev. E* **93**, 032104 (2016).
- [47] M. Rigol, V. Dunjko, and M. Olshanii, *Nature (London)* **452**, 854 (2008).
- [48] E. V. H. Doggen, I. V. Gornyi, and D. G. Polyakov, *Phys. Rev. B* **103**, L100202 (2021).
- [49] V. Khemani, M. Hermele, and R. Nandkishore, *Phys. Rev. B* **101**, 174204 (2020).
- [50] P. Sala, T. Rakovszky, R. Verresen, M. Knap, and F. Pollmann, *Phys. Rev. X* **10**, 011047 (2020).
- [51] T. Hartmann, F. Keck, H. J. Korsch, and S. Mossmann, *New J. Phys.* **6**, 2 (2004).
- [52] E. E. Mendez, F. Agulló-Rueda, and J. M. Hong, *Phys. Rev. Lett.* **60**, 2426 (1988).
- [53] A. C. Phillips, *Introduction to Quantum Mechanics* (John Wiley & Sons, Hoboken, NJ, 2013).
- [54] A. R. Kolovsky, *Phys. Rev. Lett.* **101**, 190602 (2008).
- [55] I. García-Mata and D. L. Shepelyansky, *Eur. Phys. J. B* **71**, 121 (2009).
- [56] D. Emin and C. F. Hart, *Phys. Rev. B* **36**, 7353 (1987).
- [57] T. Giamarchi, *Quantum Physics in One Dimension* (Clarendon, Oxford, 2003), Vol. 121.
- [58] T. Matsubara and H. Matsuda, *Prog. Theor. Phys.* **16**, 569 (1956).
- [59] M. Brockmann, B. Wouters, D. Fioretto, J. D. Nardis, R. Vlijm, and J.-S. Caux, *J. Stat. Mech.* (2014) P12009.
- [60] S. R. White, *Phys. Rev. Lett.* **69**, 2863 (1992).
- [61] M. Dolfi, B. Bauer, S. Keller, A. Kosenkov, T. Ewart, A. Kantian, T. Giamarchi, and M. Troyer, *Comput. Phys. Commun.* **185**, 3430 (2014).
- [62] R. Yao, T. Chanda, and J. Zakrzewski, *Ann. Phys.* **435**, 168540 (2021), Special Issue on Localisation, 2020.
- [63] L. Zhang, Y. Ke, W. Liu, and C. Lee, *Phys. Rev. A* **103**, 023323 (2021).
- [64] C. Cheng and R. Mondaini, *Phys. Rev. A* **94**, 053610 (2016).
- [65] A. B. Harris, *J. Phys. C* **7**, 1671 (1974).
- [66] J. T. Chayes, L. Chayes, D. S. Fisher, and T. Spencer, *Phys. Rev. Lett.* **57**, 2999 (1986).
- [67] J. Yu, N. Sun, and H. Zhai, *Phys. Rev. Lett.* **119**, 225302 (2017).
- [68] C. Klöckner, C. Karrasch, and D. M. Kennes, *Phys. Rev. Lett.* **125**, 147601 (2020).